International Journal of Particle Therapy 14 (2024) 100636

Contents lists available at ScienceDirect

International Journal of Particle Therapy

journal homepage: www.sciencedirect.com/journal/ijpt

Evaluation of Pelvic MRI-to-CT Deformable Registration for Adaptive MR-Guided Particle Therapy

Rita Pestana (MSc)[1,2,3,*], Katharina Seidensaal (MD)[1,2], Cedric Beyer (MSc)[1,2], Jürgen Debus (MD, PhD)[1,2,4,5], Sebastian Klüter (PhD)[1,2], Julia Bauer (PhD)[1,2]

[1] National Center for Radiation Research in Oncology (NCRO), Heidelberg Institute for Radiation Oncology (HIRO), Heidelberg, Germany
[2] Department of Radiation Oncology and Heidelberg Ion Beam Therapy Center (HIT), Heidelberg University Hospital, Heidelberg, Germany
[3] Ruprecht-Karls-Universität Heidelberg, Heidelberg, Germany
[4] National Center for Tumor Diseases (NCT), NCT Heidelberg, a partnership between DKFZ and Heidelberg University Hospital, Heidelberg, Germany
[5] German Cancer Research Center (DKFZ) Heidelberg, Clinical Cooperation Unit Radiation Oncology, Heidelberg, Germany

ARTICLE INFO

Keywords:
Adaptive therapy
Particle therapy
Magnetic resonance
Imaging
Deformable image registration

ABSTRACT

Purpose: We aim to assess the magnetic resonance imaging (MRI)-to-CT deformable image registration (DIR) quality of our treatment planning system in the pelvic region as the first step of an online MRI-guided particle therapy clinical workflow.

Materials and Methods: Using 2 different DIR algorithms, ANAtomically CONstrained Deformation Algorithm (ANACONDA), the DIR algorithm incorporated in RayStation, and Elastix, an open-source registration software, we retrospectively assessed the quality of the deformed CT (dCT) generation in the pelvic region for 5 patients. T1- and T2-weighted daily control MRI acquired prior to treatment delivery were used for the DIR. We compared the contours automatically mapped on the dCT against the manual contours on the MRI (ground truth) by calculating the Dice similarity coefficients and mean distances to the agreement for organs at risk, targets, and outer contour. We assessed the dosimetric impact of the DIR on the clinical treatment plans, comparing the dose-volume histograms and the value of the clinical goals achieved for each dCT. The water equivalent path lengths and dose range 80% (R80%) maps were compared by casting on the beams' eye view.

Results: The T1 sequences performed better for the DIR with ANACONDA compared against the T2. ANACONDA's performance agreed with Elastix. The bladder and rectum led to the worst agreement. For the remaining structures analyzed, Dice similarity coefficients above 0.80 were obtained. Maximum median deviations of 7.1 and 2.1 mm were observed for water equivalent path lengths and R80%, respectively, on the PTV.

Conclusion: This work shows a good agreement on the DIR quality achieved with ANACONDA for the structures in the beams' path. By comparing the R80% generated with ANACONDA and Elastix, we give a first quantification of the uncertainties to be considered in an online MRI-guided particle therapy workflow for pelvic treatment.

Introduction

Particle therapy (PT) treatment plans are highly sensitive to anatomical changes, due to the steep dose fall-off behind the Bragg peak and due to the strong dependence of the charged particle's range on the stopping power ratio (SPR). As a consequence, considerable safety planning margins are set around the clinical target volume, compromising the dosimetric benefit of the irradiation.[1,2] These margins can be reduced with the use of image-guided therapy.[3]

Magnetic resonance imaging (MRI) is a potential candidate for daily image guidance, offering superior soft tissue contrast without ionizing radiation. However, it does not give SPR information, required for dose calculations,[2] and a daily CT (dCT) has to be generated.

Several dCT generation methods are available, such as segment-based, atlas-based, segmentation-based, sequence-based, and methods using machine learning.[4] For radiation therapy with photons, MRI-guided therapy is already successfully used in the clinic routine with several commercial machines available,[5-9] and guidelines on the dCT

This work was previously presented at the 62nd PTCOG Annual Conference in Singapore.

* Corresponding author.
E-mail address: Rita.NetoPestana@med.uni-heidelberg.de (R. Pestana).

https://doi.org/10.1016/j.ijpt.2024.100636
Received 20 August 2024; Received in revised form 22 October 2024; Accepted 12 November 2024

accuracy required have been published.[10] Despite that, MRI-guided PT is not yet clinically implemented, and no indication exists of the required dCT accuracy.

At the Heidelberg Ion-beam Therapy Center (HIT) efforts are being made to implement an online MRI-guided adaptive workflow: A pretreatment anatomical verification MRI in immobilized position is acquired with a dedicated MRI device located outside the treatment room, and the patient is subsequently transferred via a shuttle system to the irradiation place. The pelvic region is one of the potential candidates for this workflow due to anatomy changes in the bladder, bowel, and rectum filling,[11] and also due to changes in the muscle tension or the soft tissue in the beam path. In particular, chordomas, chondrosarcomas, osteosarcomas, and soft tissue sarcomas located in the pelvic region are among the candidates for MRI-guided adaptive therapy.

The first step in the MRI-guided workflow is the generation of the dCT from the MRI. With the goal to establish a clinical workflow at HIT, an atlas-based method was chosen to perform a deformable image registration (DIR) between the planning CT and the daily MRI. This method is available in RayStation, the treatment planning system used at HIT.

DIR has a main role in the MRI-guided adaptive workflow, and it is crucial to accurately assess its quality. One common approach to this is a comparison to an independent algorithm.[12] The DIR quality between CT and MRI in the pelvic region has been assessed for several software, such as the commercial Velocity from Varian and the open-source software Elastix.[12,13] However, there is a lack of precision studies for DIR with the algorithm incorporated into RayStation, ANAtomically CONstrained Deformation Algorithm (ANACONDA).[14]

With this work, we aim to close the gap in the clinical implementation of ANCONDA in the pelvic region by presenting a study of the MRI-to-CT DIR quality achieved with this algorithm. We assessed the uncertainties in the structures' deformation for different MRI sequences by comparing the contours generated with the vector field (VF) against those manually contoured on the daily MRI (ground truth). Furthermore, we compared how ANACONDA performs against an independent algorithm (Elastix) and studied the impact of the uncertainties of the DIR algorithm choice on the clinical treatment plan.

Methods

Patient cohort and data sets

For this study, 28 pelvic patients were identified who received daily MRI. From this cohort, 5 patients fulfilled the requirement of comparable MR imaging sequences and were thus considered for the present study. The treatment plans and imaging data were anonymized and retrospectively analyzed. All analyses were performed following institutional guidelines and the Declaration of Helsinki of 1975 in its most recent version. Ethics approval for the study was granted by the Heidelberg University ethics committee (No. S-589/2023). Table 1 contains a summary of the treatment plan parameters for the 5 patients, as well as the number of daily MRI acquired for each of them and the diagnoses. The MRI was acquired at a diagnostic device (Siemens SOLA, B_0 = 1.5 T) installed at HIT, prior to the treatment delivery and with the patient in treatment position. For the patients with several daily MRIs, only the first set of examinations was used. The PTV was created by expanding the CTV by a margin between 6 and 7 mm, depending on the irradiation depth. All the plans have 2 beams, and the optimization technique used was single-field uniform dose optimization.

Planning CT images were acquired with a resolution of 0.98 × 0.98 × 3 mm^3. The daily MR imaging protocol contained 4 different sequences: a T2 turbo spin echo sequence with the Periodically Rotated Overlapping ParallEL Lines with Enhanced Reconstruction (Propeller)/blade technique and 3 T1 3D gradient echo sequences with the 2-point Dixon technique: 1 opposed-phase sequence (T1-opp), 1 in-phase sequence (T1-in), and a fat-phase sequence (T1-F), obtained by extracting the opposed-phase from the in-phase sequence. The T2 sequence features a time to echo of 114 ms and a repetition time of 2500 ms, while the T1 sequences have time to echo values of 2.33 ms (in-phase) and 4.39 ms (opposed-phase), with a repetition time of 6.8 ms. All sequences were sampled with a resolution of 1.04 × 1.04 × 3 mm^3 with 3D distortion correction applied.

Image registration

Image registration with ANACONDA was performed in a research version of RayStation 11B. We started by performing a frame of reference image registration from the planning CT to the daily MRI, followed by a rigid registration based on gray-level information. Then, a DIR with mutual information as the similarity measure was performed with ANACONDA.[14] With the VF from the DIR, the dCT was created, and the structures were deformed. The treatment couch was copied from the planning CT to the dCT without deformation.

Image registration with Elastix,[15,16] an open-source registration software, was performed in Slicer.[17] First, we performed a rigid registration between the MRI and the planning CT, using the default settings from Elastix in Slicer. After that, we performed the DIR using 2 different presets: *generic* and CT/MR-based pseudo-CT, further referred to as *pelvis*. The first preset has the default parameter settings, using mutual information and bending energy penalty as similarity measures, while the second only uses mutual information metrics (similar to ANACONDA).

Deformable image registration quality evaluation

Several sets of structures were involved in the study. The planning CT images have the corresponding structure sets contoured by the

Table 1
Information regarding the treatment plan prescribed for the 5 patients included in the study.

Patient	Ion	Prescription	No. of beams	Optimization technique	Beam's direction (°)	Average WEPL (cm)	No. of control MRI	Diagnose
1	Carbon	3 Gy × 22 fractions = 66 Gy (RBE)	2	SFUD	160 200	9.4 9.0	1	Sacrococcygeal chordoma
2	Carbon	3 Gy × 20 fractions = 66 Gy (RBE)	2	SFUD	160 200	10.4 7.4	1	Extraskeletal myxoid chondrosarcoma
3	Protons	1.8 Gy × 28 fractions = 50.40 Gy (RBE)	2	SFUD	160 200	13.4 10.7	4	Ewing sarcoma
4	Carbon	3 Gy × 22 fractions = 66 Gy (RBE)	2	SFUD	160 200	11.8 13.8	2	Sacrococcygeal chordoma
5	Protons	2 Gy × 27 fractions = 54 Gy (RBE)	2	SFUD	200 160	9.3 8.6	1	BCOR-CCNB3-fusion-positive Sarcoma

Abbreviations: MRI, magnetic resonance imaging; RBE, relative biological effectiveness; SFUD, single-field uniform dose optimization; WEPL, water equivalent path lengths.

clinicians before the treatment plan design. The dCT contains the structures automatically mapped from the planning CT with the VF. Furthermore, the structures on the daily MRI (ground truth) were manually contoured and checked by an attending radiation oncologist.

For the DIR quality evaluation, the Dice similarity coefficients (DSC)[18] and mean distances to agreement (MDA)[19] were calculated between the structures on the dCT and on the daily MRI (ground truth). Targets as well as bone and soft tissue structures were considered: gross tumor volume (GTV), clinical tumor volume (CTV), bladder, rectum, femoral heads (left and right), outer contour, and bowel. The outer contour was cropped in the sagittal direction, and only a region containing the planning tumor volume (PTV) plus a margin of up to 10 cm was considered. As for the bowel, only the region around the intersection of this structure with the PTV plus a margin of 2 cm around it was studied; for 2 of the 5 patients, there was no intersection of the bowel with this region; thus, only the remaining 3 patients were included in the bowel analysis.

In RayStation, DSC and MDA were calculated with the function SimilarityForRigidlyMappedRoiGeometry. For Elastix, DSC and MDA were calculated in Slicer using the segment comparison module, embedded in the SlicerRT extension. The consistency between the 2 implementations was verified. A schematic representation of the conducted registration quality assessment is presented in Figure 1. Figure 1 includes an illustrative dose distribution, obtained for the first patient in the study. The dose distributions for all the patients are reported in the Supplementary Material.

Assessment of dosimetric impact

To study the dosimetric impact of the DIR uncertainties, a forward dose calculation of the delivered clinical treatment plan was performed on the dCT using RayStation. The dose-volume histograms (DVHs) obtained from calculations on the dCT images generated with ANACONDA and Elastix were compared against each other and against the planning CT images. The value of the clinical goals achieved for each examination was also compared, and the relative difference in the value obtained with ANACONDA and Elastix was calculated as follows:

$$\Delta V = \frac{|V_E - V_A|}{(V_E + V_A)/2}$$

where V_E and V_A represent the values of the clinical goal obtained with Elastix and ANACONDA, respectively.

A ray cast algorithm was implemented in Python to cast either CT images or dose cubes. The algorithm was based on the method proposed by Siddon.[20] The water equivalent path lengths (WEPL) on the dCT generated with ANACONDA and Elastix were compared by casting on the beams' eye view. Casts through the dose cubes obtained from treatment plan forward calculation on the different dCT images yielded the dose range of 80% (R80%) maps. This was used to detect dose fall-off differences between the dCT generated with ANACONDA and Elastix.

Results

Deformable image registration output

Figure 2 shows an example of 2 of the MRI sequences used for each patient, as well as the corresponding dCT generated with ANACONDA. For each examination on the left-hand side, the structures manually contoured on the MRI (full line), and the structures mapped with the corresponding VF (planning CT to respective MRI) obtained with ANACONDA (dashed line) are displayed.

Deformable image registration accuracy

The results of the DSC and MDA calculated for the dCT generated with ANACONDA for the different MRI sequences studied are reported in the upper part of Figure 3. For the DSC, the values obtained for the T2 sequence ranged between 0.62 (bladder) and 0.99 (outer contour). For the same sequence, MDA values between 0.43 mm (femoral head right) and 9.7 mm (bladder) were obtained. For the T1 sequences, the minimum DSC was obtained for the rectum with the T1-opp (0.70), while the maximum was verified for the outer contour with the same sequence (0.98); MDA values ranged between 1.0 mm (femoral head right with the T1-F sequence) and 5.6 mm (bladder with the T1-F sequence).

The results obtained with ANACONDA and the 2 Elastix presets for the T1-opp MRI sequence are shown in the lower part of Figure 3. The results from Elastix *generic* range from DSC of 0.64 (bladder) to 0.96 (outer contour), whereas for the MDA, the values are comprehended between 1.26 mm (femoral head right) and 6.72 mm (bladder). For the *pelvis* preset, DSC values between 0.64 (bladder) and 0.96 (outer contour) were obtained; the MDA values ranged from 0.74 mm (GTV) to 6.67 mm (bladder).

In Figure 3, the average values of the DSC and MDA are plotted. For detailed data with all individual patient values, please refer to Appendix A, where comprehensive tables are presented.

Assessment of dosimetric impact

The DVH for one of the patients included in the study is shown in Figure 4. The plot on the left reports the dose values calculated on the planning CT (full line) and on the dCT generated with ANACONDA (dashed line) and Elastix *pelvis* (dotted line) for the T1-opp sequence. The plot on the right includes the scenarios defined by a robust evaluation of the clinical treatment plan on the planning CT set using a patient positioning and range uncertainties of 3 mm and 3%, respectively. The DVH for the other patients is available in the Supplementary Material.

For the same patient, the comparison of the clinical goals' values is presented in Table 2. Table 2 contains the clinical goals for all the region of interest (ROI) for which the DIR accuracy was evaluated. Reported are the values of the clinical goals achieved on the planning CT and on the dCT created with ANACONDA and Elastix *pelvis* for the T1-

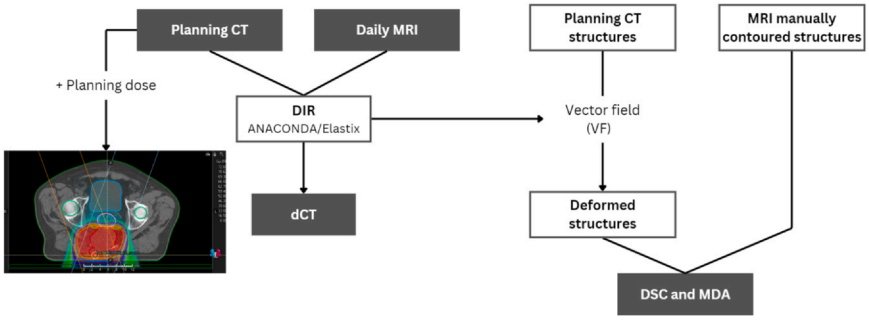

Figure 1. Schematic representation of the procedure followed to perform and evaluate the DIR quality. The left part of the scheme contains information about the image sets, whereas the right side represents the structure sets. Abbreviations: ANACONDA, ANAtomically CONstrained Deformation Algorithm; dCT, deformed CT; DIR, deformable image registration; and MDA, mean distances to agreement.

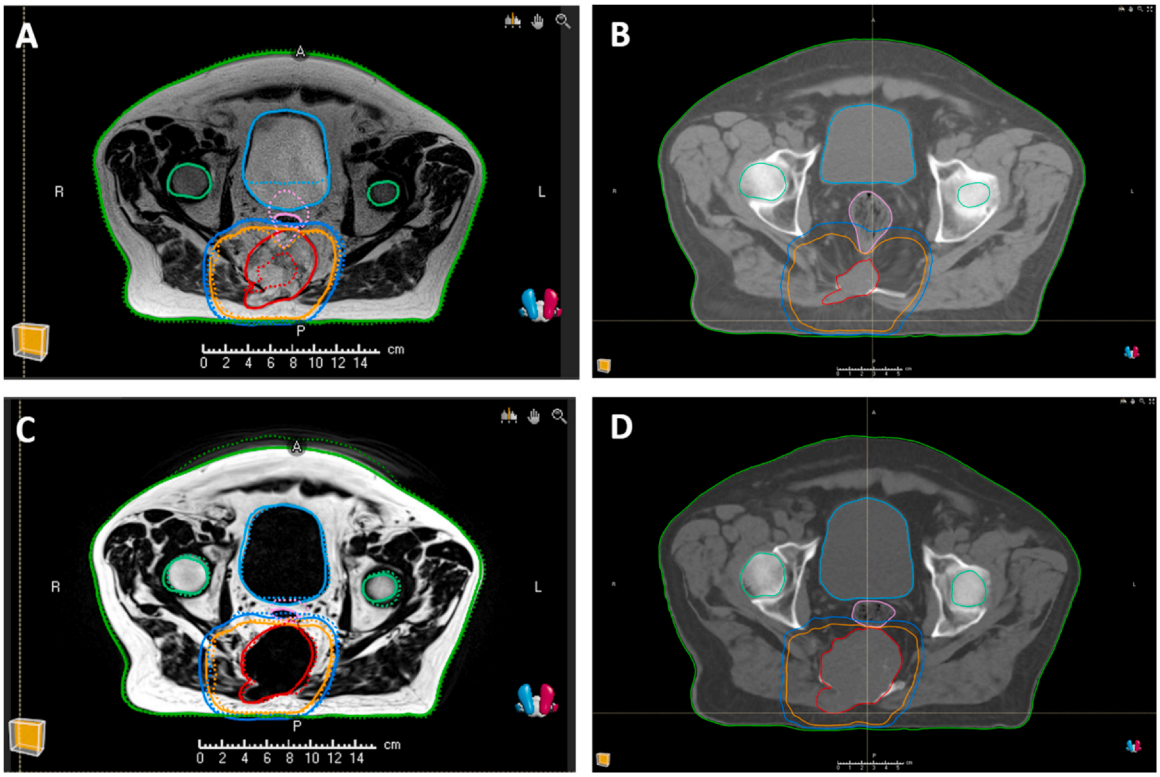

Figure 2. On the left, the MRI sequences T2 (A) and T1-opp (C) from the first patient included in the study are presented. On the right side, the dCT generated from the T2 (B) and T1-opp (D) sequences is shown. On the MRI, the structures manually contoured are represented with a full line, and the structures are automatically mapped with ANACONDA on the corresponding dCT with a dashed line. On the dCT, only the structures mapped with the VF are represented. The following structures are shown GTV (red), CTV (orange), PTV (dark blue), rectum (pink), bladder (light blue), femoral heads (dark green) and outer contour (green). Abbreviations: ANACONDA, ANAtomically CONstrained Deformation Algorithm; CTV, clinical tumor volume; dCT, deformed CT; GTV, gross tumor volume; PTV, planning tumor volume; and VF, vector field.

opp MRI sequence, as well as the value that arises from the worst scenario of the robust evaluation mentioned above. The last column contains the relative difference between the values achieved with ANACONDA and Elastix, ΔV. The Supplementary Material contains the tables with the clinical goals' values obtained for the other patients. Taking all the patients into account, the maximum difference achieved for the coverage goals was 2.3% for the CTV and 2.7% for the PTV. For the rectum and for the bowel, there was a volume clinical goal for 1 patient for which no volume on the Elastix dCT was receiving the maximum dose set by the goal. In this case, the value of the clinical goal calculated on ANACONDA's dCT was 0.13 cm^3 for the bowel and 0.34 cm^3 for the rectum. For the other patients, the maximum relative difference was 10.6% for the bowel and 5.9% for the rectum.

As for the WEPL, the whole patient depth was casted on the beam's eye view. We obtained median values ranging between −1.3 mm and 7.1 mm on the WEPL comparison between ANACONDA and Elastix on the CTV, when considering both beams for all the patients. This represents relative differences ranging up to 2.4% when compared against the maximum WEPL obtained for each beam's direction. Analysis of the R80% maps yielded minimum and maximum median deviations of −2.1 mm and 0.0 mm on the CTV, respectively. It is worth mentioning that one of the patients was not included in the dosimetric comparison, as the MRI image stack was smaller and did not include the whole target volume. For this patient, the CTV was cropped to fit into the image stack and to be used for the WEPL analysis. Illustrative plots of the WEPL and R80% comparison between ANACONDA and Elastix are shown in Appendix B.

Discussion

In this work, we assessed the DIR quality achieved with ANACONDA for different MRI sequences in an absolute fashion, by comparing mapped structures to a manually contoured ground truth, and in a relative fashion, by comparing it against Elastix. With the comparison of the structures mapped with the VF against the ground truth, we made an absolute geometrical assessment of the DIR accuracy. Moreover, we assessed the dosimetric impact of the DIR algorithm on the treatment plan prescribed for each of the 5 patients by comparing the DVH and clinical goals' values calculated on the dCT generated with ANACONDA and Elastix. Besides, we compared the WEPL and R80% maps by ray casting on beams' eye view on both dCT.

The DIR quality achieved with ANACONDA for the different MRI sequences presented significant differences for the GTV and bladder: for the bladder, the T2 MRI sequence presented a DSC of 0.62 ± 0.29 and a MDA of (9.6 ± 21.9) mm, against a DSC of 0.75 ± 0.15 and a MDA of (4.6 ± 4.7) mm achieved with the T1-opp sequence. The uncertainties on DSC and MDA were higher for the T2 sequence on the GTV and bladder, due to higher deviations between the results from the several patients. In Figure 2A and C, one can see that, unlike the T1 sequences, the T2 sequence did not reproduce the different bladder filling between the planning CT and the daily MRI for this patient. Furthermore, the automatically mapped GTV on this sequence had a significant offset when compared to the ground truth. For the different sequences, the bony structures on the dCT matched well with the daily MRI, with DSC values ranging from 0.91 to 0.98 and MDA between 0.6 and 1.4 mm for the femoral heads. For the outer contour, we also obtained good agreement, with a DSC of 0.98 ± 0.02 and a MDA of (1.4 ± 3.6) mm for the T1-opp sequence. The realistic deformation of the outer contour is relevant for the irradiation, as it strongly affects the WEPL along the beam path. The various T1 sequences performed similarly, so we decided to use the T1-opp for the comparison against Elastix.

Elastix *pelvis* led to higher DSC and lower MDA values, performing better than Elastix *generic*. ANACONDA performed comparably for most

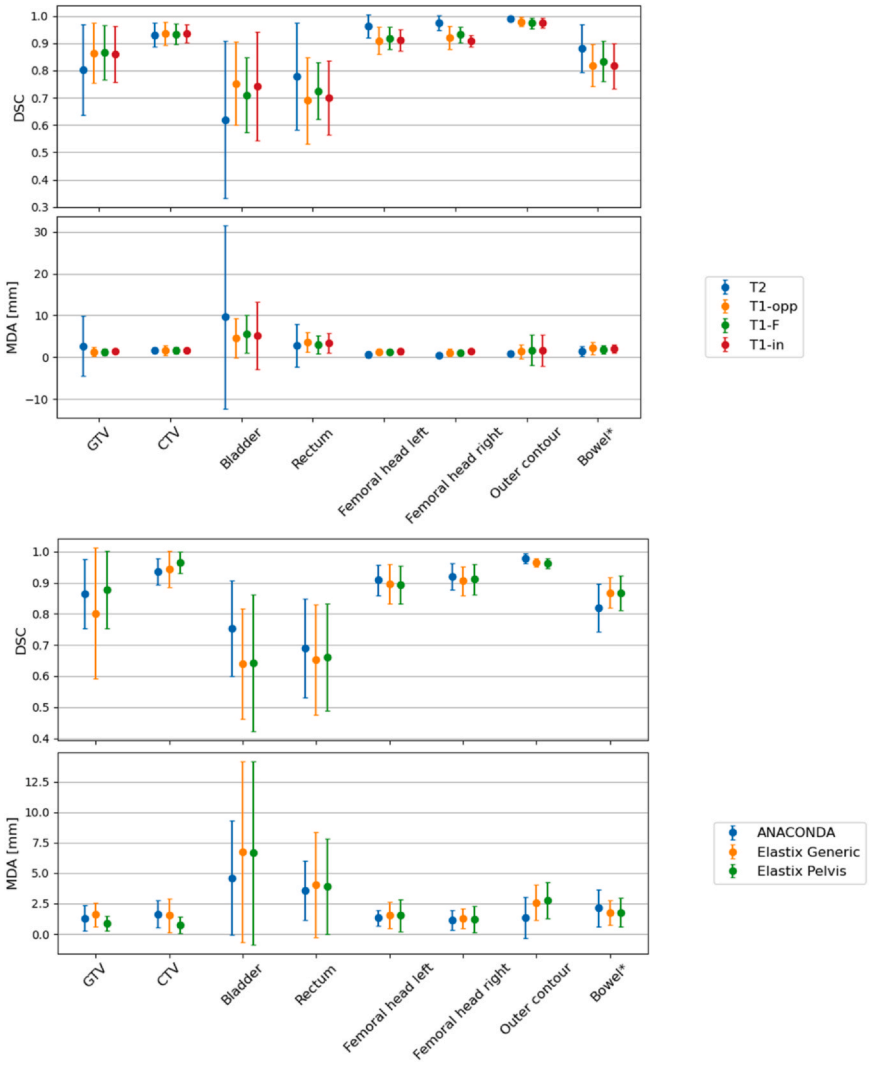

Figure 3. The upper plots report the DSC and MDA calculated between the structures manually contoured on the MRI and those automatically mapped on the dCT generated with ANACONDA for the different MRI sequences. The lower plots display the results from the dCT generated with ANACONDA, and 2 Elastix presets for the T1-opp MRI sequence. The results are averaged over the 5 patients included in the study. For the bowel, only the intersection of this structure with the PTV +2 cm was considered, and the results are the average for the 3 patients for which this intersection was verified. The error bars represent the statistical uncertainty of the mean, calculated with the DSC and MDA obtained for all the patients. Abbreviations: ANACONDA, ANAtomically CONstrained Deformation Algorithm; CTV, clinical tumor volume; dCT, deformed CT; DSC, Dice similarity coefficients; GTV, gross tumor volume; MDA, mean distances to agreement; MRI, magnetic resonance imaging; and PTV, planning tumor volume.

of the structures but presented better results for the bladder and outer contour. The DSC and MDA values are in accordance with those obtained in previous studies, for instance, in the work done by Ishida et al[12] with Elastix and the commercial software Velocity AI. The authors also found that the T1 sequence led to better results for the bladder for most Elastix settings. In the lack of reference DSC and MDA guideline values for PT, we can compare the obtained results against the guidelines from the American Association of Physicists in Medicine Task Group[10] for radiation therapy with photons, which suggest DSC values above 0.80 and MDA values below 3 mm. Except for the bladder

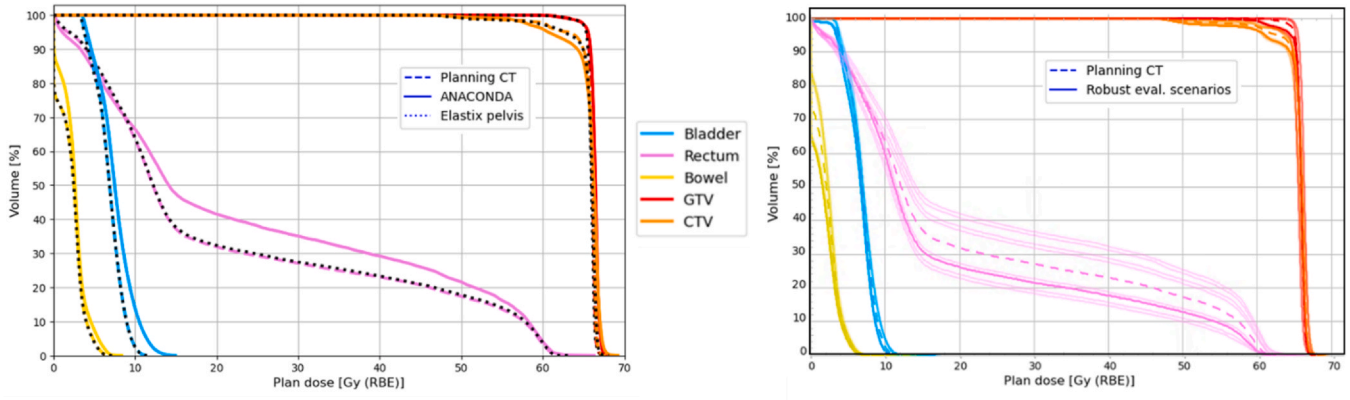

Figure 4. DVH for one of the patients included in the study. On the left DVH, 3 examinations are included as follows: planning CT (full line) and dCT generated with ANACONDA (dashed line) and Elastix *pelvis* (black dotted line). The dCT images were generated with the T1-opp MRI sequence. On the right, the scenarios defined by a robust evaluation of the planning CT set using a patient positioning and range uncertainties of 3 mm and 3%, respectively, are shown. The dashed lines represent the curves obtained on the planning CT image, whereas the full lines show each scenario. Abbreviations: ANACONDA, ANAtomically CONstrained Deformation Algorithm; CTV, clinical tumor volume; dCT, deformed CT; DVH, dose-volume histogram; GTV, gross tumor volume; and MRI, magnetic resonance imaging.

Table 2
Clinical goals' values achieved with the prescribed treatment plan on the planning CT and on the dCT obtained with ANACONDA and Elastix *pelvis* for the first patient included in the study.

ROI	Clinical goal	Planning CT	ANACONDA	Elastix *pelvis*	Worst scenario robust evaluation	ΔV
CTV	At least 95% at 62.7 Gy	95.14%	92.69%	94.87%	92.15%	2.3
PTV	At least 95% at 62.7 Gy	86.45%	82.77%	85.04%	82.24%	2.7
Bowel	At most 48 Gy at 0.03 cm^3	7.24 Gy	7.92 Gy	7.12 Gy	12.63 Gy	10.6
Rectum	At most 62.7 Gy at 0.03 cm^3	61.51 Gy	65.3 Gy	61.58 Gy	65.37 Gy	5.9

Abbreviations: ANACONDA, ANAtomically CONstrained Deformation Algorithm; CTV, clinical tumor volume; dCT, deformed CT; PTV, planning tumor volume; ROI, region of interest.
The value for the clinical goal that is obtained on the worst scenario defined by a robust evaluation on the planning CT (3 mm positioning and 3% range uncertainties, respectively) is also reported. The last column shows the relative difference between the values obtained with ANACONDA and Elastix pelvis. The dCT was generated with the T1-opp MRI sequence.

and rectum, all the organs on the dCT generated with ANACONDA met these criteria. Due to better performance, the assessment of the dosimetric impact of the DIR was done for ANACONDA against Elastix *pelvis*.

As for the dosimetric impact of the DIR algorithm choice, the DVH presented on the left side of Figure 4 shows a larger offset obtained between ANACONDA and Elastix *pelvis* for the rectum, compared against the other structures. The size of the rectum considerably decreased from the planning CT to the fraction MRI. For this structure, ANACONDA matched the shrinkage better: It led to a DSC of 0.58 and MDA of 5.0 mm, while with Elastix, we got a DSC of 0.48 and an MDA of 7.4 mm. As the dCT generated with ANACONDA contains a smaller rectum, a higher fraction of the volume receives more doses, leading to the offset seen on the DVH. Nevertheless, both DVH curves are within the uncertainties obtained from the robust evaluation scenarios defined by robust evaluation scenarios set using a patient positioning and range uncertainties of 3 mm and 3%, respectively, displayed on the right side of Figure 4. Concerning the clinical goals comparison, all the values obtained for the target structures and organs at risk on the dCT are within the tolerances defined by the same robust evaluation.

Regarding the WEPL difference between ANACONDA and Elastix, the median values on CTV ranged between −1.3 and 7.1 mm. For the R80%, median values between −2.1 and 0.0 mm were observed. The smaller difference observed on the R80% reflects the robustness of the treatment plans designed for the patients: the 2-field configuration is less sensitive to changes in patients' anatomy. Furthermore, the WEPL considers the whole patient depth, including the region behind the target volumes. These deviations represent the first quantification of the uncertainties on the beam range for sacral irradiation introduced by DIR for dCT generation. Such uncertainties need to be considered for the adaptive workflow when evaluating the treatment plan and carefully assessing the need for treatment adaptation. We can also estimate the CT-SPR uncertainty by 3% of the average WEPL of each beam, as reported in Table 1. The average WEPL ranges between 7.4 and 13.8 cm, so the CT-SPR uncertainty ranges between 2.2 and 4.1 mm. Adding this uncertainty to the maximum geometrical uncertainty we obtained due to the DIR algorithm choice (2.1 mm) leads to margins between 4.3 and 6.2 mm. This is within the PTV margins used at HIT (5-7 mm). It is worth mentioning that we can also achieve better control of the organs at risk with the adaptive workflow.

Accuracy studies for other DIR algorithms have been done with phantoms, as the work developed by Wu et al.[13] They used a physical phantom to assess the accuracy of MRI-to-MRI and MRI-to-CT DIR achieved with Velocity, from Varian, for T1 and T2 MRI sequences. Furthermore, alternative approaches have been proposed for the estimation of DIR uncertainties. A recent method, developed by Smolders et al,[21] uses neural networks to predict the uncertainties that arise from DIR. This method predicts the uncertainties of the VF and propagates them into the uncertainties on the contours and on the accumulated doses calculation. However, this uncertainty prediction method focuses on CT-to-CT registration. The application of the method on MRI-to-CT registration would require further investigation. An alternative approach for MR-only treatment planning is the generation of a synthetic CT using deep learning. At HIT, such an algorithm provided by Siemens in syngo.via[22] is currently being assessed. The accuracy of the synthetic CT will be compared against the corresponding dCT generated with ANACONDA.

The results obtained in the present study demonstrate promise, suggesting that further efforts are worth, in particular, with the goal of clinical implementation in mind. A similar analysis might be performed for other indications, for example, for patients with prostate cancer, where bony structures, the bladder, and the rectum are more in the beams path. One of the limitations of the study was the small number of patients, and this will be improved with the acquisition of further data in the future. Another constrain was the lack of a ground truth for the study of the dosimetric impact. In the absence of a daily CT, we performed a relative assessment of the dosimetric impact of the dCT generated with ANACONDA by comparing it against Elastix *pelvis*. At HIT, a patient shuttle device is currently being integrated to shuttle the patient between the MRI scanner, in-room CT, and treatment couch while being immobilized for treatment. This will allow the data acquisition for a more accurate assessment of dCT's generation impact on the dose calculation. To better assess the absolute accuracy of the DIR, a systematic study with induced deformations on a phantom is foreseen to study the impact of DIR on further indications.

Conclusion

The DIR accuracy achieved with ANACONDA against the ground truth was better for the images acquired with T1 sequences compared to the T2. Elastix *pelvis* performed better than Elastix *generic*. Furthermore, the results obtained with ANACONDA for the T1 sequences are in good agreement with Elastix *pelvis*. Good accuracy was achieved for the deformation of the outer contour with ANACONDA, a structure that strongly affects particles' range. We assessed the dosimetric impact of the DIR algorithm choice and presented a first quantification of the uncertainties introduced by DIR. Looking ahead, this study allows us to better quantify the uncertainties induced by ANACONDA's DIR, and that has to be considered in an MRI-guided adaptive PT workflow in the pelvic region.

Ethics

All analyses were performed following institutional guidelines and the Declaration of Helsinki of 1975 in its most recent version. Ethics approval for the study was granted by the Heidelberg University ethics committee (No. S-589/2023).

Funding

This work was kindly funded by the German Federal Ministry of Education and Research within the funding program “Bildgeführte

Diagnostik und Therapie—Neue Wege in der Intervention" (ARTEMIS, 13GW0436A).

Author contribution

Rita Pestana: Conceptualization, Data curation, Formal Analysis, Investigation, Methodology, Validation, Visualization, Writing – original draft. Katharina Seidensaal: Conceptualization, Formal Analysis, Methodology, Project administration, Validation, Writing – review and editing. Cedric Beyer: Data curation, Resources, Software, Validation, Writing – review and editing. Jürgen Debus: Funding acquisition, Project administration, Writing – review and editing. Sebastian Klüter: Funding acquisition, Methodology, Project administration, Validation, Writing – review and editing. Julia Bauer: Conceptualization, Formal Analysis, Funding acquisition, Investigation, Methodology, Project administration, Supervision, Validation, Writing – review and editing.

Declaration of Conflicts of Interest

The authors declare the following financial interests/personal relationships which may be considered as potential competing interests: Juergen Debus reports a relationship with RaySearch Laboratories AB that includes funding grants. Juergen Debus reports a relationship with Vision RT Ltd that includes funding grants. Juergen Debus reports a relationship with Merck Serono GmbH that includes funding grants. Juergen Debus reports a relationship with Siemens Healthcare GmbH that includes funding grants. Juergen Debus reports a relationship with PTW-Freiburg Dr Pychlau GmbH that includes: funding grants. Juergen Debus reports a relationship with Accuray Inc that includes funding grants. Juergen Debus reports a relationship with Intra OP that includes nonfinancial support. If there are other authors, they declare that they have no known competing financial interests or personal relationships that could have appeared to influence the work reported in this paper.

Acknowledgments

We thank Thomas Mielke and Beata Koczur for their technical assistance regarding the clinical treatment planning workflow. For the publication fee we acknowledge financial support by Heidelberg University.

Appendix A. Dice similarity coefficients and mean distances to agreement values

Table A1
DSC and MDA values obtained for the 5 patients included in the study.

T2	Patient 1		Patient 2		Patient 3		Patient 4		Patient 5	
ROI	DSC	MDA (cm)	DSC	MDA (cm)	DSC	MDA (cm)	DSC	MDA (cm)	DSC	MDA (cm)
GTV	0.48	0.91	0.88	0.09	0.89	0.05	0.95	0.17	0.83	0.13
CTV	0.93	0.22	0.92	0.21	0.89	0.20	0.97	0.13	0.95	0.09
Bladder	0.61	0.85	0.16	2.93	0.88	0.32	0.71	0.39	0.75	0.35
Rectum	0.49	0.74	0.95	0.05	0.92	0.09	0.81	0.18	0.73	0.37
Bowel					0.89	0.13	0.77	0.28	0.98	0.02
Femoral head left	1.00	0.00	0.91	0.12	0.99	0.01	0.96	0.07	0.95	0.09
Femoral head right	1.00	0.00	0.98	0.04	0.97	0.04	0.96	0.07	0.96	0.07
Outer contour	0.99	0.06	0.99	0.09	0.99	0.04	0.99	0.11	0.99	0.07

Abbreviations: CTV, clinical tumor volume; DSC, Dice similarity coefficients; GTV, gross tumor volume; and MDA, mean distances to agreement; ROI, region of interest.
The deformable image registration was performed with ANAtomically CONstrained Deformation Algorithm on the T2 magnetic resonance imaging sequence.

Table A2
DSC and MDA values obtained for the 5 patients included in the study.

T1-opp	Patient 1		Patient 2		Patient 3		Patient 4		Patient 5	
ROI	DSC	MDA (cm)	DSC	MDA (cm)	DSC	MDA (cm)	DSC	MDA (cm)	DSC	MDA (cm)
GTV	0.89	0.22	0.83	0.12	0.67	0.16	0.96	0.13	0.96	0.03
CTV	0.93	0.23	0.90	0.26	0.90	0.17	0.97	0.10	0.97	0.05
Bladder	0.81	0.40	0.63	0.88	0.89	0.27	0.69	0.41	0.74	0.34
Rectum	0.59	0.55	0.69	0.31	0.83	0.17	0.81	0.18	0.53	0.58
Bowel					0.91	0.12	0.65	0.39	0.90	0.13
Femoral head left	0.90	0.15	0.85	0.19	0.90	0.14	0.93	0.12	0.95	0.07
Femoral head right	0.88	0.18	0.88	0.14	0.92	0.11	0.96	0.07	0.96	0.06
Outer contour	0.96	0.29	0.99	0.05	0.99	0.07	0.99	0.10	0.97	0.18

Abbreviations: CTV, clinical tumor volume; DSC, Dice similarity coefficients; GTV, gross tumor volume; and MDA, mean distances to agreement; ROI, region of interest.
The deformable image registration was performed with ANAtomically CONstrained Deformation Algorithm on the T1-opp magnetic resonance imaging sequence.

Table A3
DSC and MDA values obtained for the 5 patients included in the study.

Generic	Patient 1		Patient 2		Patient 3		Patient 4		Patient 5	
ROI	DSC	MDA (cm)	DSC	MDA (cm)	DSC	MDA (cm)	DSC	MDA (cm)	DSC	MDA (cm)
GTV	0.89	0.23	0.72	0.21	0.51	0.25	0.99	0.03	0.89	0.08
CTV	0.92	0.28	0.92	0.27	0.93	0.13	1.00	0.02	0.95	0.07

(*continued on next page*)

Table A3 (*continued*)

Generic	Patient 1		Patient 2		Patient 3		Patient 4		Patient 5	
ROI	DSC	MDA (cm)	DSC	MDA (cm)	DSC	MDA (cm)	DSC	MDA (cm)	DSC	MDA (cm)
Bladder	0.63	0.73	0.37	1.34	0.80	0.49	0.68	0.44	0.72	0.37
Rectum	0.46	0.79	0.64	0.35	0.79	0.19	0.81	0.19	0.57	0.50
Bowel					0.92	0.10	0.78	0.29	0.90	0.13
Femoral head left	0.91	0.17	0.80	0.25	0.89	0.18	0.93	0.12	0.95	0.06
Femoral head right	0.91	0.12	0.83	0.20	0.91	0.14	0.94	0.10	0.95	0.07
Outer contour	0.96	0.25	0.95	0.39	0.97	0.19	0.98	0.21	0.96	0.25

Abbreviations: CTV, clinical tumor volume; DSC, Dice similarity coefficients; GTV, gross tumor volume; and MDA, mean distances to agreement; ROI, region of interest.

The deformable image registration was performed with Elastix generic on the T1-opp magnetic resonance imaging sequence.

Table A4

DSC and MDA values obtained for the 5 patients included in the study.

Pelvis	Patient 1		Patient 2		Patient 3		Patient 4		Patient 5	
ROI	DSC	MDA (cm)	DSC	MDA (cm)	DSC	MDA (cm)	DSC	MDA (cm)	DSC	MDA (cm)
GTV	0.93	0.13	0.87	0.10	0.67	0.14	0.99	0.03	0.94	0.04
CTV	0.95	0.14	0.96	0.11	0.95	0.07	1.00	0.02	0.97	0.04
Bladder	0.57	0.86	0.38	1.34	0.84	0.37	0.68	0.44	0.74	0.33
Rectum	0.48	0.74	0.68	0.31	0.77	0.21	0.81	0.19	0.57	0.49
Bowel					0.93	0.08	0.77	0.31	0.90	0.13
Femoral head left	0.92	0.14	0.77	0.27	0.91	0.12	0.91	0.16	0.95	0.07
Femoral head right	0.86	0.22	0.88	0.12	0.91	0.13	0.95	0.09	0.95	0.07
Outer contour	0.96	0.25	0.94	0.41	0.98	0.20	0.97	0.24	0.96	0.28

Abbreviations: CTV, clinical tumor volume; DSC, Dice similarity coefficients; GTV, gross tumur volume; and MDA, mean distances to agreement; ROI, region of interest.

The deformable image registration was performed with Elastix pelvis on the T1-opp magnetic resonance imaging sequence.

Table A5

DSC and MDA values obtained for the 5 patients included in the study.

T1-F	Patient 1		Patient 2		Patient 3		Patient 4		Patient 5	
ROI	DSC	MDA (cm)	DSC	MDA (cm)	DSC	MDA (cm)	DSC	MDA (cm)	DSC	MDA (cm)
GTV	0.90	0.20	0.83	0.11	0.69	0.15	0.96	0.15	0.95	0.03
CTV	0.92	0.24	0.92	0.20	0.89	0.19	0.97	0.14	0.97	0.06
Bladder	0.72	0.62	0.57	0.97	0.83	0.40	0.69	0.45	0.74	0.35
Rectum	0.58	0.50	0.79	0.22	0.82	0.20	0.82	0.17	0.63	0.46
Bowel					0.88	0.14	0.70	0.30	0.92	0.10
Femoral head left	0.92	0.12	0.87	0.15	0.92	0.11	0.93	0.13	0.95	0.07
Femoral head right	0.90	0.15	0.92	0.10	0.93	0.09	0.95	0.10	0.96	0.06
Outer contour	0.92	0.50	0.99	0.07	0.99	0.08	0.99	0.08	0.98	0.13

Abbreviations: CTV, clinical tumor volume; DSC, Dice similarity coefficients; GTV, gross tumor volume; and MDA, mean distances to agreement; ROI, region of interest.

The deformable image registration was performed with ANAtomically CONstrained Deformation Algorithm on the T1-F magnetic resonance imaging sequence.

Table A6

DSC and MDA values obtained for the 5 patients included in the study.

T1-inn	Patient 1		Patient 2		Patient 3		Patient 4		Patient 5	
ROI	DSC	MDA (cm)	DSC	MDA (cm)	DSC	MDA (cm)	DSC	MDA (cm)	DSC	MDA (cm)
GTV	0.92	0.16	0.81	0.13	0.70	0.15	0.95	0.17	0.92	0.07
CTV	0.93	0.21	0.93	0.18	0.90	0.18	0.97	0.14	0.95	0.09
Bladder	0.83	0.39	0.50	1.23	0.92	0.20	0.69	0.45	0.76	0.32
Rectum	0.62	0.46	0.70	0.30	0.82	0.18	0.80	0.18	0.56	0.55
Bowel					0.84	0.18	0.69	0.31	0.91	0.11
Femoral head left	0.92	0.13	0.85	0.19	0.91	0.13	0.93	0.13	0.95	0.08
Femoral head right	0.92	0.13	0.90	0.12	0.89	0.15	0.91	0.18	0.93	0.11
Outer contour	0.92	0.49	0.99	0.06	0.99	0.08	0.99	0.07	0.98	0.10

Abbreviations: CTV, clinical tumor volume; DSC, Dice similarity coefficients; GTV, gross tumor volume; and MDA, mean distances to agreement; ROI, region of interest.

The deformable image registration was performed with ANAtomically CONstrained Deformation Algorithm on the T1-in magnetic resonance imaging sequence.

Appendix B: Ray cast: WEPL and R80% maps

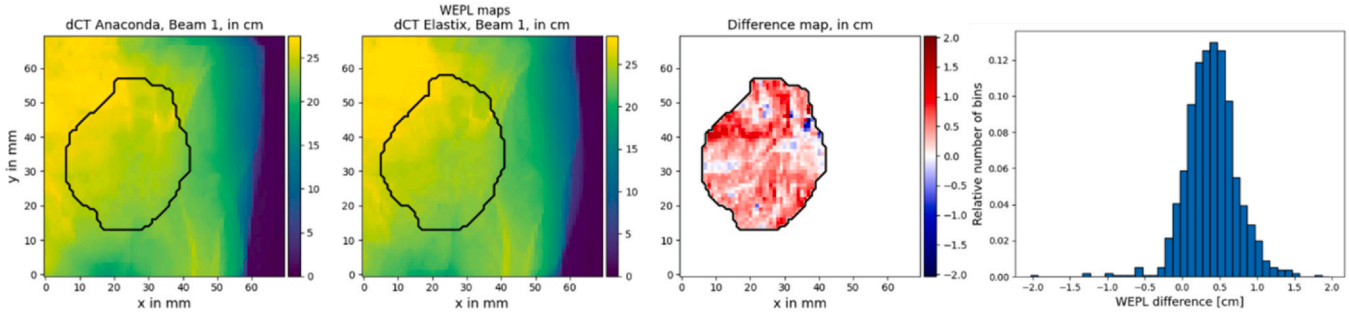

Figure B1. Illustrative WEPL maps for one of the treatments plan's beams for the first patient included in the study calculated on the dCT generated with ANACONDA (left) and with Elastix *pelvis* (center-left) with the T1-opp sequence. On the center-right, the difference on WEPL (Elastix-ANACONDA) on the CTV is shown. On the right is the histogram with the WEPL difference on the CTV. Abbreviations: ANACONDA, ANAtomically CONstrained Deformation Algorithm; CTV, clinical tumor volume; dCT, deformed CT; and WEPL, water equivalent path lengths..

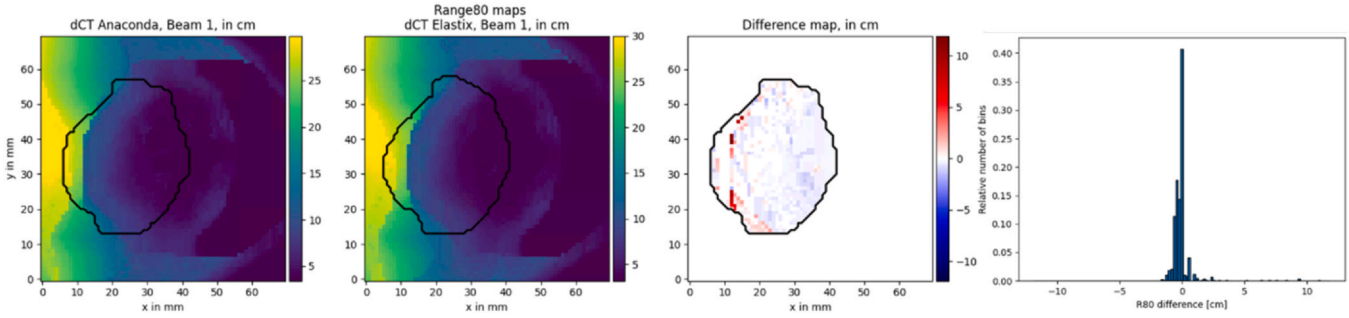

Figure B2. Illustrative R80% maps for one of the treatments plan's beams for the first patient included in the study calculated on the dCT generated with ANACONDA (left) and with Elastix *pelvis* (center-left) with the T1-opp sequence. On the center-right, the difference on R80% (Elastix-ANACONDA) on the CTV is shown. On the right is the histogram with the R80% difference on the CTV. Abbreviations: ANACONDA, ANAtomically CONstrained Deformation Algorithm; CTV, clinical tumor volume; and dCT, deformed CT..

Appendix A. Supplementary material

Supplementary data associated with this article can be found in the online version at doi:10.1016/j.ijpt.2024.100636.

References

1. Paganetti H. Range uncertainties in proton therapy and the role of Monte Carlo simulations. *Phys Med Biol.* 2012;57(11):R99–117. https://doi.org/10.1088/0031-9155/57/11/R99
2. Hoffmann A, Oborn B, Moteabbed M, et al. MR-guided proton therapy: a review and a preview. *Radiat Oncol.* 2020;15(1):129. https://doi.org/10.1186/s13014-020-01571-x
3. Landry G, Hua C-H. Current state and future applications of radiological image guidance for particle therapy. *Med Phys.* 2018;45(11):e1086–e1095. https://doi.org/10.1002/mp.12744
4. Nenoff L, Amstutz F, Murr M, et al. Review and recommendations on deformable image registration uncertainties for radiotherapy applications. *Phys Med Biol.* 2023;68(24):24TR01. https://doi.org/10.1088/1361-6560/ad0d8a
5. Werensteijn-Honingh AM, Kroon PS, Winkel D, et al. Feasibility of stereotactic radiotherapy using a 1.5 T MR-linac: multi-fraction treatment of pelvic lymph node oligometastases. *Radiother Oncol.* 2019;134:50–54. https://doi.org/10.1016/j.radonc.2019.01.024
6. Dawson LA, Sharpe MB. Image-guided radiotherapy: rationale, benefits, and limitations. *Lancet Oncol.* 2006;7(10):848–858. https://doi.org/10.1016/s1470-2045(06)70904-4
7. Corradini S, Alongi F, Andratschke N, et al. MR-guidance in clinical reality: current treatment challenges and future perspectives. *Radiat Oncol.* 2019;14(1):92. https://doi.org/10.1186/s13014-019-1308-y
8. Acharya S, Fischer-Valuck BW, Kashani W, et al. Online magnetic resonance image guided adaptive radiation therapy: first clinical applications. *Int J Radiat Oncol Biol Phys.* 2016;94(2):394–403. https://doi.org/10.1016/j.ijrobp.2015.10.015
9. Pollard JM, Wen Z, Sadagopan R, et al. The future of image-guided radiotherapy will be MR guided. *Br J Radiol.* 2017;90(1073):20160667. https://doi.org/10.1259/bjr.20160667
10. Brock KK, Mutic S, McNutt TR, et al. Use of image registration and fusion algorithms and techniques in radiotherapy: report of the AAPM Radiation Therapy Committee Task Group No. 132. *Med Phys.* 2017;44(7):e43–e76. https://doi.org/10.1002/mp.12256
11. Eminowicz G, Motlib J, Khan S, et al. Pelvic organ motion during radiotherapy for cervical cancer: understanding patterns and recommended patient preparation. *Clin Oncol (R Coll Radiol).* 2016;28(9):e85–91. https://doi.org/10.1016/j.clon.2016.04.044
12. Ishida T, Kadoya N, Kadoya N, Tanabe S, et al. Evaluation of performance of pelvic CT-MR deformable image registration using two software programs. *J Radiat Res.* 2021;62(6):1076–1082. https://doi.org/10.1093/jrr/rrab078
13. Wu RY, Liu AY, Yang J, et al. Evaluation of the accuracy of deformable image registration on MRI with a physical phantom. *J Appl Clin Med Phys.* 2020;21(1):166–173. https://doi.org/10.1002/acm2.12789
14. Weistrand O, Svensson S. The ANACONDA algorithm for deformable image registration in radiotherapy. *Med Phys.* 2015;42(1):40–53. https://doi.org/10.1118/1.4894702
15. Klein S, Staring M, Murphy K, et al. elastix: a toolbox for intensity-based medical image registration. *IEEE Trans Med Imaging.* 2010;29(1):196–205. https://doi.org/10.1109/TMI.2009.2035616
16. Shamonin DP, Bron EE, Lelieveldt BPF, et al. Fast parallel image registration on CPU and GPU for diagnostic classification of Alzheimer's disease. *Front Neuroinform.* 2013;7:50. https://doi.org/10.3389/fninf.2013.00050
17. Fedorov A, Beichel R, Kalpathy-Cramer J, et al. 3D slicer as an image computing platform for the quantitative imaging network. *Magn Reson Imaging.* 2012;30(9):1323–1341. https://doi.org/10.1016/j.mri.2012.05.001
18. Dice LR. Measures of the amount of ecologic association between species. *Ecology.* 1945;26(3):297–302. https://doi.org/10.2307/1932409
19. Chalana V, Kim Y. A methodology for evaluation of boundary detection algorithms on medical images. *IEEE Trans Med Imaging.* 1997;16(5):642–652. https://doi.org/10.1109/42.640755
20. Siddon RL. Fast calculation of the exact radiological path for a three-dimensional CT array. *Med Phys.* 1985;12(2):252–255. https://doi.org/10.1118/1.595715
21. Smolders A, Lomax A, Weber DC, Albertini F. Deep learning based uncertainty prediction of deformable image registration for contour propagation and dose accumulation in online adaptive radiotherapy. *Phys Med Biol.* 2023;68(24):245027. https://doi.org/10.1088/1361-6560/ad0282
22. Hoesl M, Corral NE, Mistry N. MR-based Synthetic CT reimagined. An AI-based algorithm for continuous Hounsfield units in the pelvis and brain – with *syngo*.via RT Image Suite (VB60).